THE PHOTOGRAMMETRIC RECORD

The Photogrammetric Record 26(135): 339–360 (September 2011)
DOI: 10.1111/j.1477-9730.2011.00648.x

CALIBRATION OF LONG FOCAL LENGTH CAMERAS IN CLOSE RANGE PHOTOGRAMMETRY

CHRISTOS STAMATOPOULOS (xstamatopoulos@gmail.com)
CLIVE S. FRASER (c.fraser@unimelb.edu.au)
University of Melbourne, Australia

Abstract

One of the practical impediments to the adoption of long focal length lenses in close range photogrammetry is the difficulty in network exterior orientation and self-calibration that can be encountered with the collinearity equation model when the camera field of view is smaller than around 10°. This paper reports on an investigation that examined two different avenues for improving the self-calibration of long focal length cameras. The first is a re-examination of the linearisation of the collinearity equations with additional calibration parameters, and especially determination of the coefficients in the design matrix corresponding to the interior orientation elements. The second is a new approach to the calculation of object space coordinates by employing an orthogonal projection model that can be formulated as a bundle adjustment with self-calibration. Accuracy aspects of both approaches are discussed and test cases employing both zoom and macro lenses are presented.

KEYWORDS: automatic camera calibration, bundle adjustment, close range photogrammetry, long focal length lenses, macro lenses, orthogonal projection, self-calibration, zoom lenses

INTRODUCTION

CLOSE RANGE PHOTOGRAMMETRY, as the name suggests, has been traditionally limited to short to medium camera-to-object distances. With the growing use of off-the-shelf digital SLR cameras for photogrammetric measurement, however, there are emerging requirements to perform measurements over: (a) long distances, for applications in construction engineering, deformation monitoring and traffic accident reconstruction; as well as (b) very short distances for applications such as digital documentation and 3D visualisation of cultural heritage objects via image-based approaches. Such measurements often require the use of long focal length lenses both to keep the spatial resolution high and to optimise the angular measurement precision. It has long been recognised that there can be practical impediments to the adoption of very long focal length lenses on small format cameras, these centring principally upon potential difficulties in analytical orientation and, consequently, self-calibration. As focal length increases, so the field of view becomes narrower. This can impact adversely on the

performance of the conventional central perspective, collinearity equation model, since the bundle of rays can approach, in effect, a parallel projection.

Fully automatic camera self-calibration generally employs object point arrays in which some, or all, of the targeted points are coded. The data processing is nowadays a ''push one button'' operation and, so long as well-known principles such as convergent imaging, the use of orthogonal camera roll angles and, desirably, use of a 3D target distribution are adopted, a successful outcome can be anticipated for medium- and wide-angle lenses. In applying network orientation with self-calibration to images with very narrow fields of view, however, problems can arise through over-parameterisation, ill-conditioning and subsequent numerical instability in the normal equations of the bundle adjustment. The appearance of numerical problems might be expected when the field of view drops below 10° (Stamatopoulos et al., 2010), which is equivalent to a 200 mm lens on a 35 mm format digital SLR camera. The recovery of satisfactory camera calibration parameters is often precluded in such ''weak geometry'' cases due to linear dependencies that arise between the interior and exterior orientation parameters.

The non-linearity of the collinearity equations is considered an inherent obstacle when it comes to the self-calibration of long focal length lenses, since deterioration of the linear independence of the interior and exterior orientation parameters can be anticipated. This partially accounts for why recent research on this topic has been focused more on the development of alternative linear models to accommodate such network geometries. For example, Ono and Hattori (2002) developed an orthogonal projection model to address the issue of long distance measurements in close range photogrammetry. Even though their model was successful, it had limitations in that the calibration of interior orientation elements was ignored and object space control points were required for the calculation of the initial exterior orientation parameters. For the measurement of small objects, Rova et al. (2008) implemented a parallel projection model that requires parallel projection images taken with telecentric lenses, the bundle adjustment incorporating a simplified interior orientation model. For either of these two cases, a fully automatic self-calibration procedure was precluded.

The development of an automated calibration process for consumer grade digital cameras with long focal length lenses forms the topic of this paper, the aim of the development being twofold: firstly, to improve the robustness and precision of recovery of camera interior and exterior orientation parameters, and secondly, to extend the applicability of self-calibration to cameras with fields of view as narrow as a few degrees.

In seeking to overcome problems encountered in the self-calibration of cameras with lenses of very long focal length, two prospective approaches have been adopted, one centred on the traditional collinearity equations and one on an orthogonal projection model. In the first approach, a re-examination of the traditional linearisation of the collinearity equations with additional parameters is carried out to reveal shortcomings that manifest themselves when long focal length lenses are employed. The second approach centres on the development of an alternative, orthogonal projection model that is better suited to the ''difficult'', and invariably weaker, geometries encountered in photogrammetric networks employing cameras with very narrow fields of view. Under the orthogonal projection model, a fully automatic camera calibration via bundle adjustment with self-calibration is again possible.

CAMERA CALIBRATION MODEL

The well-known eight-parameter ''physical'' camera calibration model developed by Brown (1971) has been found to be almost universally applicable in close range photogrammetry. For long focal length lenses, however, a careful selection of parameters

has to be performed, especially as the correlation between interior and exterior orientation parameters increases with increasing focal length. The photogrammetric properties of long focal length lenses are well recognised and have previously been noted by Fryer and Fraser (1986), Wiley and Wong (1995), Noma et al. (2002), Labe and Förstner (2004) and Fraser and Al-Ajlouni (2006).

The calculation of the principal distance and the principal point coordinates is of equal importance for both long and short focal length lenses, in spite of the opportunities for projective compensation in the photogrammetric orientation of narrow field of view imagery. Also, the radial distortion is metrically very significant and needs to be taken into account for any photogrammetric application. Radial distortion is universally modelled via the well-known odd-ordered polynomial expression comprising terms to the seventh order. However, for zoom lenses the third-order coefficient K_1 is usually sufficient to describe the radial distortion profile. The maximum radial distortion occurs at the minimum zoom focal length and for lenses exhibiting only barrel distortion it decreases as the zoom focal length increases. For many zoom lenses there will be a zero crossing between the barrel distortion at short focal lengths and the pincushion distortion at long focal lengths (Fraser and Al-Ajlouni, 2006).

The image coordinate correction model adopted for self-calibration of long focal length lenses can then comprise the quite familiar four-parameter subset of Brown's model:

$$\begin{aligned} x_{corr} &= x - x_p + (x - x_p)K_1 r^2 - \frac{x}{c} dc \\ y_{corr} &= y - y_p + (y - y_p)K_1 r^2 - \frac{y}{c} dc \end{aligned} \tag{1}$$

where c is the principal distance and r is the radial distance, with

$$r = \sqrt{(x - x_p)^2 + (y - y_p)^2}.$$

Central Perspective Model

Partial Derivatives

Upon linearisation of the collinearity equations to form the configuration matrix **A** of the observation equations for the bundle adjustment, partial derivatives with respect to the unknown calibration parameters forming equation (1) are determined. Traditionally, this has yielded coefficients of -1 for the parameters x_p and y_p, resulting in a model that has served the photogrammetric community well for over 40 years. However, given the impact of even the smallest inaccuracies in the ill-conditioned, and consequently unstable, equation system for the self-calibrating bundle adjustment that can arise when cameras with very long focal lengths are involved, it is right to look again at the determination of the partial derivatives of the image correction model, especially the terms for the principal point coordinates.

The well-known collinearity equations can be given in the form

$$\begin{pmatrix} x_{corr} \\ y_{corr} \end{pmatrix} = -c \begin{pmatrix} U/W \\ V/W \end{pmatrix} \tag{2}$$

where

$$U = r_{11}(X - X_o) + r_{12}(Y - Y_o) + r_{13}(Z - Z_o)$$
$$V = r_{21}(X - X_o) + r_{22}(Y - Y_o) + r_{23}(Z - Z_o)$$
$$W = r_{31}(X - X_o) + r_{32}(Y - Y_o) + r_{33}(Z - Z_o)$$

with r_{ij} being the elements of the rotation matrix **R**. Traditionally, the partial derivative terms of the collinearity equations with respect to the calibration parameters of equation (1) in the configuration matrix **A** are as follows:

$$\begin{array}{c} \\ \partial x \\ \partial y \end{array} \begin{array}{c} \begin{array}{cccc} c & x_p & y_p & K_1 \end{array} \\ \begin{pmatrix} \frac{-U}{W} & -1 & 0 & (x - x_p)r^2 \\ \frac{-V}{W} & 0 & -1 & (y - y_p)r^2 \end{pmatrix} \end{array}.$$

However, the more correct representation, taking account of the partial differentiation with respect to parameters x_p and y_p, is as the follows:

$$\begin{array}{c} \\ \partial_x \\ \partial_y \end{array} \begin{array}{c} \begin{array}{ccccc} c & & x_p & & y_p & & K_1 \end{array} \\ \begin{pmatrix} \frac{-U}{W} & & -1 - K_1 r^2 - 2\bar{x}^2 K_1 & & -2K_1 \bar{x}\bar{y} & & \bar{x}r^2 \\ \frac{-V}{W} & & -2K_1 \bar{x}\bar{y} & & -1 - K_1 r^2 - 2\bar{y}^2 K_1 & & \bar{y}r^2 \end{pmatrix} \end{array}$$

where $\bar{x} = x - x_p$ and $\bar{y} = y - y_p$.

It will be shown that this small expansion or correction to the configuration matrix can greatly enhance the recovery of the interior orientation parameters in the self-calibration of cameras with long focal length lenses, even though the magnitude of K_1 might only be of the order of 10^{-5}. In situations where the correlation between camera parameters is not high, the presence of small errors in the coefficients of the **A** matrix might not have a significant impact upon interior orientation parameter estimation, and consequently upon the exterior orientation and object space coordinates. However, the opposite can be true where there is strong projective coupling, as with narrow field of view imagery.

Even though a four-parameter correction model has been selected as appropriate for long focal length lenses, it is always possible to add further lens distortion parameters. For most lenses, the additional parameters will not lead to increased accuracy. However, in cases where the additional parameters are warranted, the partial derivatives of the principal point offset will involve additional terms, calculated as shown above.

Orthogonal Projection Model

The mathematical formulation of the orthogonal projection model can be presented in two steps. The first is the derivation of the more generic affine model and the second is formulation of the orthogonal projection model. This orthogonal projection formulation, which can be cast as a bundle adjustment, is quite rigorous in the sense that it is derived from the central perspective model and it is thus more than a simple empirical formulation. Such a relationship does not exist between the affine model and the perspective model in the absence of additional constraints.

Derivation of the Orthogonal Projection Model

Under the central perspective, collinearity equation model commonly used in close range photogrammetry, the projection of an object point into its corresponding image point is given by

$$\begin{bmatrix} x \\ y \\ -c \end{bmatrix} = \lambda \begin{bmatrix} r_{11} & r_{12} & r_{13} \\ r_{21} & r_{22} & r_{23} \\ r_{31} & r_{32} & r_{33} \end{bmatrix} \begin{bmatrix} X - X_o \\ Y - Y_o \\ Z - Z_o \end{bmatrix} \tag{3}$$

where λ is the scale factor, c the principal distance, r_{ij} the elements of the rotation matrix and X_o, Y_o, Z_o the coordinates of the perspective centre. The scale factor λ is an unknown value which varies for each object point. If λ is substituted by a constant scale parameter s, equation (3) can be rewritten as

$$\frac{s}{\lambda} \begin{bmatrix} x \\ y \\ -c \end{bmatrix} = \begin{bmatrix} x_a \\ y_a \\ -\frac{s}{\lambda} c \end{bmatrix} = s \begin{bmatrix} r_{11} & r_{12} & r_{13} \\ r_{21} & r_{22} & r_{23} \\ r_{31} & r_{32} & r_{33} \end{bmatrix} \begin{bmatrix} X - X_o \\ Y - Y_o \\ Z - Z_o \end{bmatrix} \tag{4}$$

and, by moving X_o, Y_o, Z_o to the left-hand side, equation (4) can be recast as

$$\begin{bmatrix} x_a - X'_o \\ y_a - Y'_o \\ -\frac{s}{\lambda} c - Z'_o \end{bmatrix} = s \begin{bmatrix} r_{11} & r_{12} & r_{13} \\ r_{21} & r_{22} & r_{23} \\ r_{31} & r_{32} & r_{33} \end{bmatrix} \begin{bmatrix} X \\ Y \\ Z \end{bmatrix} \tag{5}$$

where

$$\begin{bmatrix} X'_o \\ Y'_o \\ Z'_o \end{bmatrix} = -s \begin{bmatrix} r_{11} & r_{12} & r_{13} \\ r_{21} & r_{22} & r_{23} \\ r_{31} & r_{32} & r_{33} \end{bmatrix} \begin{bmatrix} X_o \\ Y_o \\ Z_o \end{bmatrix}. \tag{6}$$

The first and second rows of equation (5) express the affine projection model:

$$\begin{bmatrix} x_a \\ y_a \end{bmatrix} = s \begin{bmatrix} r_{11} & r_{12} & r_{13} \\ r_{21} & r_{22} & r_{23} \end{bmatrix} \begin{bmatrix} X \\ Y \\ Z \end{bmatrix} + \begin{bmatrix} X'_o \\ Y'_o \end{bmatrix}. \tag{7}$$

This model requires the transformation from central perspective image coordinates to affine coordinates, an operation that will be discussed later. The number of independent parameters is eight and, geometrically, the eight orientation parameters for an affine image are considered to be three image rotations, two translation elements X'_o, Y'_o the image scale s and two rotation parameters describing the relationship between projected rays and the normal to the image plane. By generalising equation (7), the collinearity equations' equivalents for the affine projection model are derived as

$$\begin{aligned} x_a &= A_1 X + A_2 Y + A_3 Z + A_4 \\ y_a &= A_5 X + A_6 Y + A_7 Z + A_8. \end{aligned} \tag{8}$$

The affine projection model allows oblique projection to an image plane. The addition to equation (8) of constraints for orthogonal projection then leads to the orthogonal projection model. Because the generalised coefficients A_i, are derived from the components r_{ij} of the rotation matrix and the scale parameter s, they should have the following properties of an orthogonal rotation matrix:

The vectors $\mathbf{a}_x = (A_1, A_2, A_3)$ and $\mathbf{a}_y = (A_5, A_6, A_7)$ must be perpendicular to each other and thus the dot product $\mathbf{a}_x \cdot \mathbf{a}_y$ has to be zero. This will force the rays from the object to be orthogonal to the image plane, such that

$$A_1 A_5 + A_2 A_6 + A_3 A_7 = 0. \tag{9}$$

The norms of $\mathbf{a}_x$ and $\mathbf{a}_y$ must be equal, meaning that the scale in the x_a direction is equivalent to that in the y_a direction, so that

$$A_1^2 + A_2^2 + A_3^2 = A_5^2 + A_6^2 + A_7^2. \tag{10}$$

The difference between the affine and orthogonal projection models is that the latter allows only perpendicular projection to an image plane. The orthogonal projection model has six independent parameters. The two constraints of equations (9) and (10) reduce the degrees of freedom of equation (8) from eight to six. More precisely, the principal distance and a distance from the projection centre to the object point along the optical axis are replaced by a uniform scale factor. The distinction between the position of the principal point and the horizontal position of the projection centre with respect to the image plane then becomes meaningless. This situation can be visualised by letting the projection centre approach an infinite position along the optical axis.

Transformation from Central Perspective to Affine Projection Coordinates

It has been recognised (Hattori et al., 2000; Ono and Hattori, 2002; Fraser and Yamakawa, 2004) that for both the affine and orthogonal projection models to be applicable, an initial conversion from a central perspective to an affine image is warranted. It has been stated that in very narrow fields of view this can be avoided, since the subsequent accuracy loss will be minimal. The image coordinate transformation is the same for both the affine and the orthogonal projection models.

Although mathematically any value can be assigned to the scale factor s, the application of an orthogonal projection to a frame camera becomes more realistic when the scale factor is calculated in a specific way. From a practical point of view, s is adjusted so as to scale down the average photographing distance to the same length as the principal distance, as shown in Fig. 1.

If H is the average photographic distance in the Z direction so that $H = \bar{Z} - Z_o$, then s can be calculated as follows:

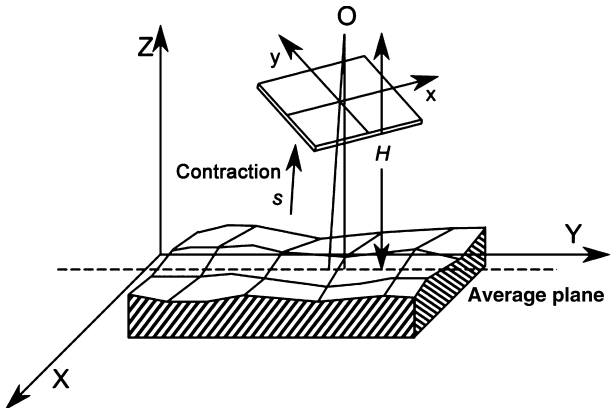

FIG. 1. The constant scale parameter s.

$$s = -\frac{r_{33}c}{\bar{Z} - Z_o} = -\frac{r_{33}c}{H}. \tag{11}$$

Equation (3) can be recast as

$$\begin{bmatrix} X - X_o \\ Y - Y_o \\ Z - Z_o \end{bmatrix} = \frac{1}{\lambda} \begin{bmatrix} r_{11} & r_{21} & r_{31} \\ r_{12} & r_{22} & r_{32} \\ r_{13} & r_{23} & r_{33} \end{bmatrix} \begin{bmatrix} x \\ y \\ -c \end{bmatrix} \tag{12}$$

and the third row of equation (12) can then be used to calculate λ as

$$\lambda = \frac{r_{13}x + r_{23}y - r_{33}c}{Z - Z_o}. \tag{13}$$

By substituting equations (11) and (13) into (4), the expressions for transforming from central perspective image coordinates to affine coordinates are obtained:

$$\begin{aligned} x_a &= \frac{Z - Z_o}{H} \frac{r_{33}c}{(r_{33}c - r_{13}x - r_{23}y)} x \\ y_a &= \frac{Z - Z_o}{H} \frac{r_{33}c}{(r_{33}c - r_{13}x - r_{23}y)} y. \end{aligned} \tag{14}$$

Additionally, the calibration model of equation (1) can be incorporated into the transformation:

$$\begin{aligned} x_a &= \frac{Z - Z_o}{H} \frac{r_{33}c}{(r_{33}c - r_{13}x_{corr} - r_{23}y_{corr})} x_{corr} \\ y_a &= \frac{Z - Z_o}{H} \frac{r_{33}c}{(r_{33}c - r_{13}x_{corr} - r_{23}y_{corr})} y_{corr}. \end{aligned} \tag{15}$$

Relationship between Orientation Parameters of the Central Perspective and Orthogonal Projection Models

The orthogonal projection model is a rigorous model that derives from the central perspective model. Therefore, it is possible to determine the relationship of the exterior orientation parameters between the two models. From the definition of the orthogonal projection model it is known that:

$$\begin{bmatrix} A_1 & A_2 & A_3 \\ A_5 & A_6 & A_7 \end{bmatrix} = s \begin{bmatrix} r_{11} & r_{12} & r_{13} \\ r_{21} & r_{22} & r_{23} \end{bmatrix}. \tag{16}$$

Since the norm of each of the vectors $\vec{\mathbf{r_1}} = (r_{11}, r_{12}, r_{13})$ and $\vec{\mathbf{r_2}} = (r_{21}, r_{22}, r_{23})$ is equal to 1, then

$$s^2 = A_1^2 + A_2^2 + A_3^2. \tag{17}$$

From equations (10) and (16) the elements of $\vec{\mathbf{r_1}}$ and $\vec{\mathbf{r_2}}$ are easily determined. The vector $\vec{\mathbf{r_3}} = (r_{31}, r_{32}, r_{33})$ can be estimated by considering the geometric features of the rotation matrix:

$$r_{11}^2 + r_{21}^2 + r_{31}^2 = 1$$

so that:

$$r_{31} = \pm\sqrt{1 - r_{11}^2 - r_{21}^2}.$$

Similarly:

$$r_{32} = \pm\sqrt{1 - r_{12}^2 - r_{22}^2}$$

$$r_{33} = \pm\sqrt{1 - r_{13}^2 - r_{23}^2}.$$

Additionally, from the properties of the rotation matrix:

$$r_{11}r_{31} + r_{12}r_{32} + r_{13}r_{33} = 0$$
$$r_{21}r_{31} + r_{22}r_{32} + r_{23}r_{33} = 0.$$

If c is given, Z_o can be calculated from equation (11) as

$$Z_o = \frac{r_{33}c}{s} + \bar{Z}. \tag{18}$$

The following expression is then obtained from the general formula of the affine model and via equation (6):

$$\begin{bmatrix} A_4 \\ A_8 \end{bmatrix} = -\begin{bmatrix} A_1 & A_2 & A_3 \\ A_5 & A_6 & A_7 \end{bmatrix} \begin{bmatrix} X_o \\ Y_o \\ Z_o \end{bmatrix}. \tag{19}$$

If the above equations are solved for X_o, Y_o, then the location of the perspective centre is obtained as

$$\begin{aligned} Y_o &= \frac{A_1A_8 - A_4A_5 - A_3A_5Z_o + A_1A_7Z_o}{A_2A_5 - A_1A_6} \\ X_o &= -\frac{A_4 + A_2Y_o + A_3Z_o}{A_1}. \end{aligned} \tag{20}$$

In cases where the parameters of the central perspective model are known, calculation of the A_i parameters of the orthogonal projection model using equations (11) and (16) is quite straightforward. Equation (11), however, requires some prior knowledge of the object point coordinates. In the case that this calculation needs to be performed at the initial stage of the bundle adjustment, approximate values are required. The determination of these approximate object point coordinates will be explained in the following section.

PHOTOGRAMMETRIC ORIENTATION PROCEDURE

Based on the algorithms presented, a complete, automated photogrammetric orientation procedure can be formulated. Various steps are involved in the process of calculating initial

approximate values, as well as at every iteration of the bundle adjustment. The procedure is summarised in the flowchart of Fig. 2.

This process for the bundle adjustment based on the orthogonal projection model is distinct from previously reported methods, which have tended to concentrate on experimental verification of the appropriateness of the model. For example, in the approach of Ono and Hattori (2002), initial approximate values for the object point coordinates needed to have been measured by non-photogrammetric means, namely, ground survey via a total station. Perturbed values of these coordinates were then used to calculate approximate values of the orthogonal

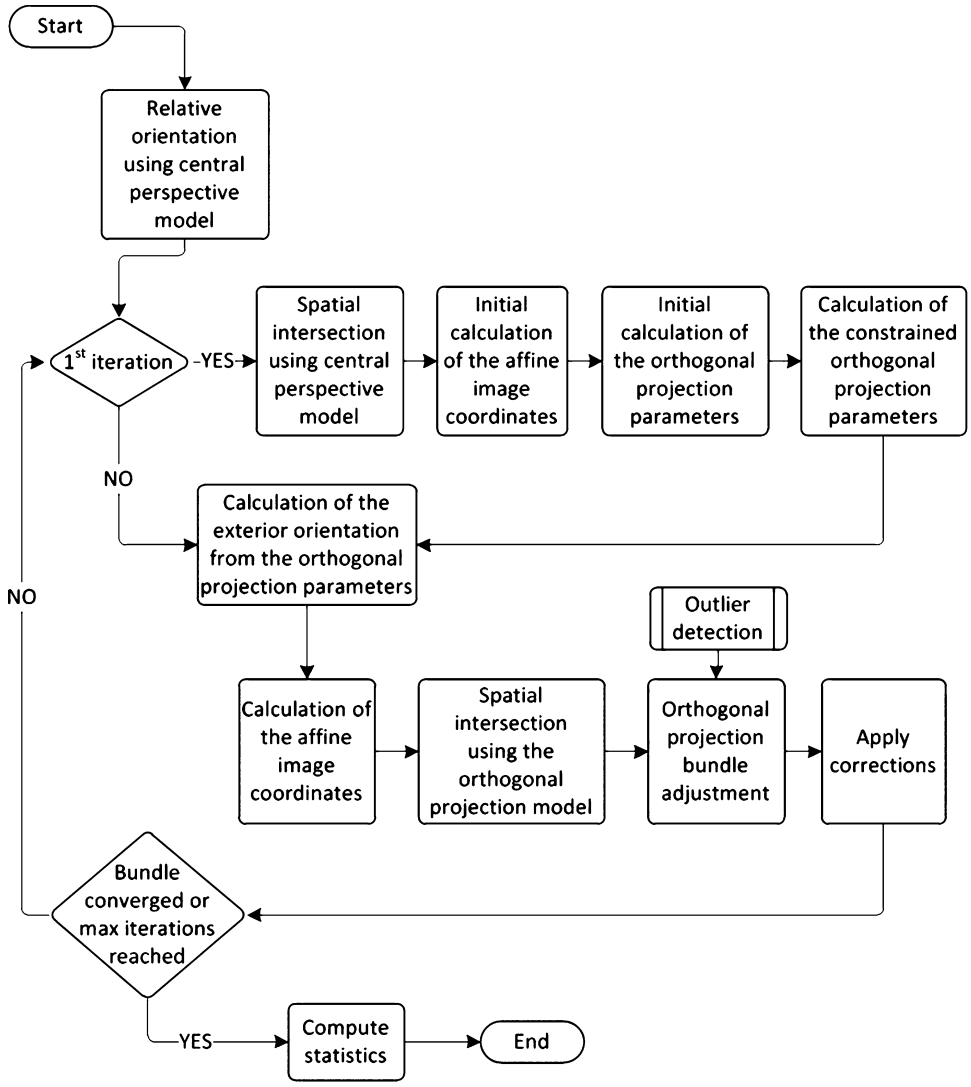

FIG. 2. Flowchart for automated orientation procedure based on the orthogonal projection model.

projection orientation parameters via a direct linear transformation (DLT), which itself is prone to instability and even numerical singularity when employed for computing the exterior orientation of long focal length lenses.

The procedure developed here is more closely related to the typical close range photogrammetric methodology, where exterior orientation is carried out using imagery alone, without the provision of any externally measured object point coordinate information. First, a relative orientation is performed between selected images using conventional, perspective model-based coplanarity equations (Cronk et al., 2006; Luhmann et al., 2006). Approximate exterior orientation parameters $(\omega, \phi, \kappa, X_o, Y_o, Z_o)$ and object point coordinates (X, Y, Z) are then obtained for the remaining images in the network via resection and spatial intersection.

The next stage involves the calculation of orientation parameters of the orthogonal projection model. Affine image coordinates are first computed, after which there is a determination of the parameters of the affine projection model. The optimal approach for the recovery of the affine orientation parameters is via a least squares adjustment in which the unknown parameters A_i in the linear system of equation (8) are computed. A subsequent least squares adjustment with the orthogonal projection constraints contained in equations (9) and (10) is then performed in order to acquire the orientation parameters of the orthogonal projection model.

Once the orthogonal orientation parameters are known, the equivalent central perspective parameters can be updated in order to reflect the current values of the orthogonal projection model. This step is significant mostly for the calculation of both Z_o and the rotation elements that are involved in the transformation of the central perspective coordinates to their corresponding affine values. Despite the fact that the rest of the exterior orientation parameters are not used in the orthogonal projection model, they are nevertheless needed in order to visualise the results since it is not possible to conceptualise an orthogonal space as a Euclidean subspace. Additionally, a final refinement in the transformation of the central perspective to affine coordinates is performed once all the parameters are known.

Even though the orthogonal projection model is quite similar to the central perspective model, as has been illustrated by Ono and Hattori (2002), some differences can be expected due to the adjustment procedures involved. Thus, a spatial intersection process using the orthogonal projection model is carried out in order to refine the object point coordinates. The authors' experience is that by doing so the subsequent bundle adjustment converges in fewer iterations.

Two bundle adjustment cases are now considered, the first being the simpler case without self-calibration, and the second being where the calibration parameters forming equation (1) are included.

Bundle Adjustment without Self-calibration

In the simpler case of the orthogonal projection model that is formulated as shown in equation (8), the form of the normal equations does not differ from that of the perspective model. The linearised form of the model can be expressed as

$$\mathbf{A}_1\mathbf{x}_1 + \mathbf{A}_2\mathbf{x}_2 = \mathbf{b} \tag{21}$$

where $\mathbf{x}_1$ represents the sensor exterior orientation parameters and $\mathbf{x}_2$ the object point coordinates. The $\mathbf{A}_i$ matrices are the corresponding configuration matrices and $\mathbf{b}$ is the image coordinate discrepancy vector. The corresponding normal equations for a network of m photos containing n measured points in the object space then follow as

$$\begin{bmatrix} \mathbf{N}_{11} & \mathbf{N}_{12} \\ \mathbf{N}_{12}{}^{\mathbf{T}} & \mathbf{N}_{22} \end{bmatrix} \begin{bmatrix} \hat{\mathbf{x}}_1 \\ \hat{\mathbf{x}}_2 \end{bmatrix} = \begin{bmatrix} \mathbf{c}_1 \\ \mathbf{c}_2 \end{bmatrix} \tag{22}$$

where $\mathbf{N}_{ij}$ and $\mathbf{c}_i$ represent contributions arising solely from the image coordinate observations, $\hat{\mathbf{x}}_1$ is an $8m \times 1$ vector of corrections to the elements of exterior orientation $(A_1, A_2, A_3, A_4, A_5, A_6, A_7, A_8)$ and $\hat{\mathbf{x}}_2$ is a $3n \times 1$ vector of corrections to the coordinates of object points (X, Y, Z). For the calculation of the elements of matrices $\mathbf{N}_{ij}$, the partial derivatives of equation (8) with respect to the unknown parameters are computed with the resulting configuration matrix being

$$\mathbf{A} = [\mathbf{A}_1 | \mathbf{A}_2] = \left[\begin{array}{cccccccc|ccc} X & Y & Z & 1 & 0 & 0 & 0 & 0 & A_1 & A_2 & A_3 \\ 0 & 0 & 0 & 0 & X & Y & Z & 1 & A_5 & A_6 & A_7 \end{array}\right].$$

The two constraints contained in equations (9) and (10) have to be accounted for with the orthogonal projection model. This can be achieved either by bordering the normal equation matrix of equation (22) and solving the least squares adjustment in a two-step algorithm or, preferably, by adding the constraints to the current normal equations:

$$\begin{bmatrix} \mathbf{N}_{11} + \mathbf{H}^{\mathbf{T}}\mathbf{W}\mathbf{H} & \mathbf{N}_{12} \\ \mathbf{N}_{12}{}^{\mathbf{T}} & \mathbf{N}_{22} \end{bmatrix} \begin{bmatrix} \hat{\mathbf{x}}_1 \\ \hat{\mathbf{x}}_2 \end{bmatrix} = \begin{bmatrix} \mathbf{c}_1 - \mathbf{H}^{\mathbf{T}}\mathbf{W}\mathbf{d} \\ \mathbf{c}_2 \end{bmatrix}. \tag{23}$$

Here, $\mathbf{H}$ is the $2m \times 8m$ matrix of additional constraints, $\mathbf{d}$ the corresponding $2m \times 1$ discrepancy vector and $\mathbf{W}$ the $2m \times 2m$ matrix of weights assigned to the constraints. The matrix $\mathbf{H}$ is formed as

$$\mathbf{H} = \begin{bmatrix} 2A_1 & 2A_2 & 2A_3 & 0 & -2A_5 & -2A_6 & -2A_7 & 0 \\ A_5 & A_6 & A_7 & 0 & A_1 & A_2 & A_3 & 0 \end{bmatrix}.$$

In the general form presented by equation (23), the normal equations will be rank deficient, since an explicit definition of the object space coordinate datum has not been made, in other words no control points have been employed. In the case of the affine and orthogonal projection models, the rank deficiency is 12 (Okamoto, 1992). In order to specify the datum, additional constraints have to be introduced. Although there are a number of ways to impose the required minimal constraints, the most advantageous approach is generally considered to be the adoption of inner constraints (for example, Fraser, 1982, 1984) where the 12 linearly independent vectors of the inner constraint matrix $\mathbf{G}$ satisfy the relationship $\mathbf{AG} = \mathbf{0}$. The inner constraint matrix can be conveniently partitioned into two components, $\mathbf{G}_1$ relating to the exterior orientation parameters, and $\mathbf{G}_2$ relating to the object space coordinates, with the elements for each being

$$\mathbf{G}_1^{\mathbf{T}} = \begin{bmatrix} A_1 & 0 & 0 & 0 & A_2 & 0 & 0 & 0 & A_3 & 0 & 0 & 0 \\ 0 & A_1 & 0 & 0 & 0 & A_2 & 0 & 0 & 0 & A_3 & 0 & 0 \\ 0 & 0 & A_1 & 0 & 0 & 0 & A_2 & 0 & 0 & 0 & A_3 & 0 \\ 0 & 0 & 0 & A_1 & 0 & 0 & 0 & A_2 & 0 & 0 & 0 & A_3 \\ A_5 & 0 & 0 & 0 & A_6 & 0 & 0 & 0 & A_7 & 0 & 0 & 0 \\ 0 & A_5 & 0 & 0 & 0 & A_6 & 0 & 0 & 0 & A_7 & 0 & 0 \\ 0 & 0 & A_5 & 0 & 0 & 0 & A_6 & 0 & 0 & 0 & A_7 & 0 \\ 0 & 0 & 0 & A_5 & 0 & 0 & 0 & A_6 & 0 & 0 & 0 & A_7 \end{bmatrix}$$

and

$$\mathbf{G}_2^{\mathbf{T}} = \begin{bmatrix} -X & -Y & -Z & -1 & 0 & 0 & 0 & 0 & 0 & 0 & 0 & 0 \\ 0 & 0 & 0 & 0 & -X & -Y & -Z & -1 & 0 & 0 & 0 & 0 \\ 0 & 0 & 0 & 0 & 0 & 0 & 0 & 0 & -X & -Y & -Z & -1 \end{bmatrix}.$$

Although minimal constraints for both exterior orientation and object point coordinates have been presented for the sake of completeness, only the constraint matrix $\mathbf{G}_2$ is applied in the presented approach, in order to achieve minimum mean variance for the object space coordinates (Fraser, 1982). The bordered normal equations then take the following form, from which the solution vector $\hat{\mathbf{X}}$ and the covariance matrix $\mathbf{Q}_{\hat{\mathbf{x}}}$ can be obtained:

$$\begin{bmatrix} \mathbf{N}_{11} + \mathbf{H}^{\mathbf{T}}\mathbf{W}\mathbf{H} & \mathbf{N}_{12} & 0 \\ \mathbf{N}_{12}{}^{\mathbf{T}} & \mathbf{N}_{22} & \mathbf{G}_2 \\ 0 & \mathbf{G}_2{}^{\mathbf{T}} & 0 \end{bmatrix} \begin{bmatrix} \hat{\mathbf{x}}_1 \\ \hat{\mathbf{x}}_2 \\ \mathbf{k} \end{bmatrix} = \begin{bmatrix} \mathbf{c}_1 - \mathbf{H}^{\mathbf{T}}\mathbf{W}\mathbf{d} \\ \mathbf{c}_2 \\ 0 \end{bmatrix}. \tag{24}$$

Bundle Adjustment with Self-calibration

The complete orthogonal projection model can be found by combining equations (8), (15) and (1):

$$\begin{aligned} &\left(\frac{Z - Z_o}{H}\right)\left(\frac{r_{33}c\left(x - x_p + \left(x - x_p\right)K_1r^2\right)}{r_{33}c - r_{13}\left(x - x_p + \left(x - x_p\right)K_1r^2\right) - r_{23}\left(y - y_p + \left(y - y_p\right)K_1r^2\right)}\right)\ldots \\ &\quad \ldots \quad A_1X - A_2Y - A_3Z - A_4 = 0 \\ &\left(\frac{Z - Z_o}{H}\right)\left(\frac{r_{33}c\left(y - y_p + \left(y - y_p\right)K_1r^2\right)}{r_{33}c - r_{13}\left(x - x_p + \left(x - x_p\right)K_1r^2\right) - r_{23}\left(y - y_p + \left(y - y_p\right)K_1r^2\right)}\right)\ldots \\ &\quad \ldots \quad A_5X - A_6Y - A_7Z - A_8 = 0. \end{aligned} \tag{25}$$

This non-linear model involves both observations and unknown parameters, which necessitates linearisation to the following form for subsequent bundle adjustment:

$$\mathbf{A}_1\mathbf{x}_1 + \mathbf{A}_2\mathbf{x}_2 + \mathbf{A}_3\mathbf{x}_3 + \mathbf{B}\mathbf{v} + \mathbf{w} = 0. \tag{26}$$

Here, $\mathbf{A}_1, \mathbf{A}_2, \mathbf{A}_3$ are configuration matrices for interior and exterior orientation parameters and object point coordinates, respectively; $\mathbf{B}$ is the matrix of partial derivatives with respect to the observations; and $\mathbf{w}$ is the functional value corresponding to the approximate parameter values and observed image coordinates. The resulting normal equations for the network of l cameras and m photos containing n measured points in object space then follow as

$$\begin{bmatrix} \mathbf{N}_{11} & \mathbf{N}_{12} & \mathbf{N}_{13} \\ \mathbf{N}_{12}{}^{\mathbf{T}} & \mathbf{N}_{22} & \mathbf{N}_{23} \\ \mathbf{N}_{13}{}^{\mathbf{T}} & \mathbf{N}_{23}{}^{\mathbf{T}} & \mathbf{N}_{33} \end{bmatrix} \begin{bmatrix} \hat{\mathbf{x}}_1 \\ \hat{\mathbf{x}}_2 \\ \hat{\mathbf{x}}_3 \end{bmatrix} = \begin{bmatrix} \mathbf{c}_1 \\ \mathbf{c}_2 \\ \mathbf{c}_3 \end{bmatrix} \tag{27}$$

where the subscripts 1, 2 and 3 now relate to camera calibration parameters, exterior orientation and object point coordinates, respectively. Thus, $\hat{\mathbf{x}}_1$ is a $4l \times 1$ vector of corrections to elements of interior orientation (c, x_p, y_p, K_1), $\hat{\mathbf{x}}_2$ is an $8m \times 1$ vector of corrections to elements of exterior orientation $(A_1, A_2, A_3, A_4, A_5, A_6, A_7, A_8)$, and $\hat{\mathbf{x}}_3$ is the $3n \times 1$ vector of corrections to the point coordinates (X, Y, Z). In order to facilitate a more

straightforward calculation of partial derivatives in the linearisation of equation (25), the rotation angles r_{ij} can be expressed in terms of the orthogonal orientation parameters and considered as constants along with the term $(Z - Z_o)/H$. The linearisation of the principal point offset should use the complete form of the correction model as explained earlier, in order to obtain proper correction values. By naming the two expressions of equation (25) as f_x and f_y, the configuration matrix $\mathbf{A}$ can be presented in terms of its component matrices $\mathbf{A}_i$ as follows:

$$\begin{aligned}\mathbf{A} &= [\mathbf{A}_1|\mathbf{A}_2|\mathbf{A}_3] \\ &= \left[\begin{array}{cccc|} \frac{\partial f_x}{\partial c} & \frac{\partial f_x}{\partial x_p} & \frac{\partial f_x}{\partial y_p} & \frac{\partial f_x}{\partial K_1} \\ \frac{\partial f_y}{\partial c} & \frac{\partial f_y}{\partial x_p} & \frac{\partial f_y}{\partial y_p} & \frac{\partial f_y}{\partial K_1} \end{array}\right. \cdots \\ &\quad \cdots \left.\begin{array}{cccccccc|ccc} -X & -Y & -Z & -1 & 0 & 0 & 0 & 0 & -A_1 & -A_2 & -A_3 \\ 0 & 0 & 0 & 0 & -X & -Y & -Z & -1 & -A_5 & -A_6 & -A_7 \end{array}\right].\end{aligned}$$

The matrix of partial derivatives with respect to the observations will have the following form:

$$\mathbf{B} = \begin{bmatrix} \frac{\partial f_x}{\partial x} & \frac{\partial f_x}{\partial y} \\ \frac{\partial f_y}{\partial x} & \frac{\partial f_y}{\partial y} \end{bmatrix}.$$

The expressions for the partial derivative terms of configuration matrices $\mathbf{A}_1$ and $\mathbf{B}$ can be found in the Appendix.

In implementing the final bundle adjustment, the addition of the free network and the orthogonal projection constraints to the normal equations needs to be performed in a two-step algorithm since the constraints of equations (9) and (10) cannot be incorporated in the same way as for the bundle adjustment without additional camera calibration parameters. Instead, double bordering of the normal equation matrix is required to apply the inner and orthogonal projection constraints, the rank defect again being 12:

$$\begin{bmatrix} \mathbf{N}_{11} & \mathbf{N}_{12} & \mathbf{N}_{13} & 0 & 0 \\ \mathbf{N}_{12}^{\mathbf{T}} & \mathbf{N}_{22} & \mathbf{N}_{23} & 0 & \mathbf{H} \\ \mathbf{N}_{13}^{\mathbf{T}} & \mathbf{N}_{23}^{\mathbf{T}} & \mathbf{N}_{33} & \mathbf{G}_2 & 0 \\ 0 & 0 & \mathbf{G}_2^{\mathbf{T}} & 0 & 0 \\ 0 & \mathbf{H}^{\mathbf{T}} & 0 & 0 & 0 \end{bmatrix} \begin{bmatrix} \hat{\mathbf{x}}_1 \\ \hat{\mathbf{x}}_2 \\ \hat{\mathbf{x}}_3 \\ \mathbf{k} \\ \boldsymbol{\lambda} \end{bmatrix} = \begin{bmatrix} \mathbf{c}_1 \\ \mathbf{c}_2 \\ \mathbf{c}_3 \\ 0 \\ \mathbf{z} \end{bmatrix}. \tag{28}$$

This system of normal equations is initially solved without the orthogonal constraints being applied:

$$\hat{\mathbf{x}}_\mathbf{o} = -\mathbf{R}^{-1}\mathbf{c}$$

where

$$\mathbf{R} = (\mathbf{N} + \mathbf{G}\mathbf{G}^{\mathbf{T}}).$$

Then, the solution with the orthogonal projection constraints applied follows from

$$\begin{aligned}\mathbf{S} &= \mathbf{H}\mathbf{R}^{-1}\mathbf{H}^{\mathbf{T}} \\ \mathbf{T} &= \mathbf{R}^{-1}\mathbf{H}^{\mathbf{T}}\mathbf{S}^{-1} \\ \hat{\mathbf{x}} &= \hat{\mathbf{x}}_\mathbf{o} + \mathbf{T}(\mathbf{z} - \mathbf{H}\hat{\mathbf{x}}_\mathbf{o}).\end{aligned}$$

Finally, the covariance matrix $\mathbf{Q}_{\hat{\mathbf{x}}}$ of the adjusted parameters can be obtained from

$$\mathbf{Q}_{\hat{\mathbf{x}}} = \mathbf{R}^{-1} - \mathbf{THR}^{-1}. \tag{29}$$

EXPERIMENTAL RESULTS AND DISCUSSION

A number of photogrammetric measurements were carried out to experimentally verify the two proposed camera calibration approaches, namely, the collinearity equation model with modified partial derivatives for interior orientation elements, and the orthogonal projection model. Three test cases will be presented here, the first two involving the self-calibration of a Nikon D200 digital SLR camera, and the third the calibration of a Nikon D80 camera. Case 1 involved a zoom lens set at 300 mm (field of view of 4·5°), Case 2 employed a lens of 400 mm focal length (field of view of 3·4°) and Case 3 used a macro lens at 135 mm focal length (field of view of 10°).

Case 1—Lens of 300 mm Focal Length

The seven-station, 21-image convergent geometry of Case 1 is shown in Fig. 3, the adopted lens being a Nikon ED AF NIKKOR 70 to 300 mm zoom lens, fixed at 300 mm. Three images per station were recorded, at zero, 90° and −90° roll angles, over a camera-to-object distance of 70 m. The approximate distance between adjacent camera stations was 12 m. In both this case and Case 2, coded retroreflective targets were employed to facilitate fully automatic network exterior orientation and self-calibration. A total of 88 coded and 25 single-dot retrotargets were used in Case 1, with strobe illumination being provided by an external Nikon Speedlight SB 800 flash unit. Three such 21-image networks were recorded and processed.

Bundle adjustments with self-calibration based on the two projection models were carried out for the three networks. This allowed both a comparison of the results between the

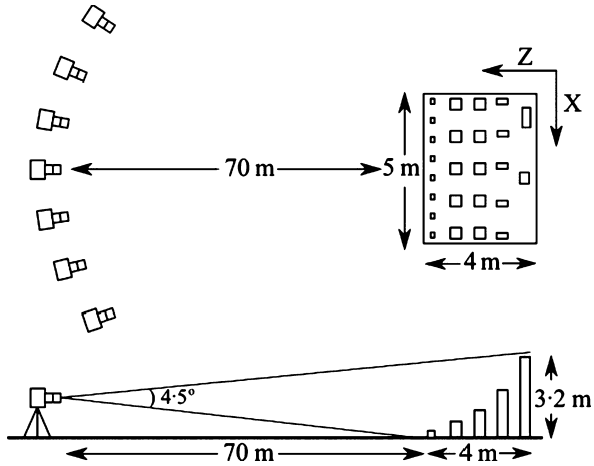

FIG. 3. Seven-station, 21-image network configuration for Case 1, using a 300 mm focal length.

TABLE I. Camera calibration results for Case 1, 300 mm lens (units are mm except for K_1).

	Perspective model		*Orthogonal projection model*	
	Values	σ	*Values*	σ
c	264·76	0·15	264·79	0·10
x_p	−0·082	0·002	−0·080	0·002
y_p	−0·295	0·003	−0·297	0·003
K_1	−6·728e−5	6·9e−8	−6·733e−5	6·5e−8

TABLE II. Precision of object point coordinates for Case 1.

	Perspective model		*Orthogonal projection model*	
σ_X	0·09 mm	1:70 000	0·07 mm	1:88 000
σ_Y	0·06 mm	1:98 000	0·06 mm	1:108 000
σ_Z	0·21 mm	1:29 000	0·20 mm	1:29 000
Mean std. error σ_{XYZ}	0·12 mm	1:51 000	0·11 mm	1:55 000
Rms of *xy* image coordinate residuals	0·83 μm		0·82 μm	

collinearity and the orthogonal projection-based models and an assessment of the degree of repeatability in the recovery of camera calibration parameters. All adjustment solutions were obtained without any numerical stability issues and the calibrations showed a high repeatability, consistent with the precision of recovery of the camera parameters. Table I lists the calibration parameters obtained in one of the networks for the collinearity model with expanded coefficients for the principal point coordinates in the configuration matrix, and for the orthogonal projection model. It is evident that both models provide essentially identical results.

The overall accuracy of object point coordinate determination for the same network is summarised in Table II, where it can be seen that the two different models yielded comparable results, with the orthogonal projection model producing marginally better accuracy in the *XY* direction.

The three networks were also solved with the conventional self-calibration model (coefficients of −1 for x_p and y_p in the **A** matrix). However, the solution was unstable and yielded implausible results for the interior orientation parameters, with estimates of the standard error for c, x_p and y_p being several millimetres. The poor determinability and repeatability of the camera interior orientation parameters also adversely impacted upon the accuracy of the computed exterior orientation and object point coordinates.

Case 2—Lens of 400 mm Focal Length

The network geometry for Case 2, illustrated in Fig. 4, was similar to that of Case 1 but with the following distinctions: the camera to object distance was 100 m; the overall convergence angle was somewhat less (7 m between adjacent stations); and the employed focal length was 400 mm, the lens being a Nikon 80 to 400 mm VR zoom lens. For this network, 94 coded and 25 single retroreflective targets were used. In addition to the primary 21-image network, a second set of 18 images was acquired from six additional stations to independently assess the integrity of the initial self-calibration, and especially to assess the stability of recovery of camera parameters. The camera stations for this second network were positioned between those of the seven-station configuration.

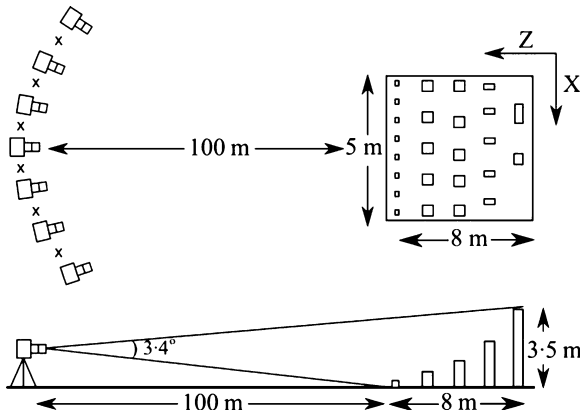

FIG. 4. Seven-station, 21-image network configuration for Case 2, with a 400 mm focal length.

Self-calibrating bundle adjustments for the perspective and orthogonal projection models were performed, these being again free of numerical stability issues. The estimates obtained for interior orientation parameters for the two networks, via either of the projection models, displayed no significant differences, even though the geometry was weaker than in Case 1 and the field of view narrower at 3·4°. For this case the recovery of a stable calibration via the collinearity equation model with a traditional additional parameter model (coefficients of −1 for x_p and y_p in the **A** matrix) was not possible, which further highlights the utility of the new approaches.

As a final processing step for Case 2, the 21- and 18-image networks were combined in a 39-image bundle adjustment in order to improve the precision of the recovery of both calibration parameters and object point coordinates. The results for this self-calibration adjustment, the camera stations of which are shown in Fig. 5, are summarised in Table III.

It is noteworthy that the 80 to 400 mm zoom lens of Case 2 had very pronounced chromatic aberration which degraded image quality and thus also the accuracy of image point centroiding. The adverse impact of chromatic aberration can be seen in the higher rms value of image coordinate residuals, and consequently also in poorer than anticipated precision of object point coordinate determination.

In regard to accuracy in object space in Case 2, the perspective and orthogonal models yielded significantly different estimates of (X, Y, Z) coordinate precision. It is apparent from Table III that the performance of the perspective model has deteriorated with the increase in

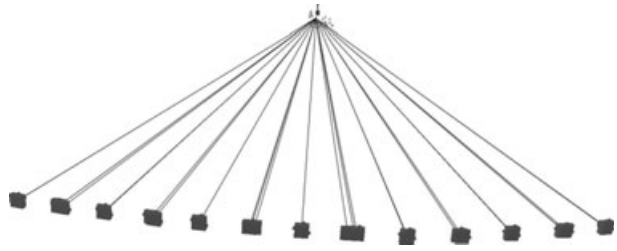

FIG. 5. Thirteen-station, 39-image network configuration for combined Case 2.

TABLE III. Precision of object point coordinates in the 39-image combined network of Case 2.

	Perspective model		*Orthogonal projection model*	
σ_X	0·12 mm	1:72 000	0·07 mm	1:132 700
σ_Y	0·30 mm	1:30 000	0·08 mm	1:117 500
σ_Z	0·54 mm	1:17 000	0·50 mm	1:17 800
Mean std. error σ_{XYZ}	0·32 mm	1:28 000	0·22 mm	1:41 600
Rms value of *xy* residuals	1·3 μm		1·3 μm	

the camera-to-object distance and the longer focal length. The orthogonal model produced markedly higher accuracy in *XY* coordinates (non-depth directions) and, perhaps as should be anticipated, its relative performance is enhanced as the field of view narrows.

Whereas numerical issues did not arise in the bundle adjustments via the proposed orthogonal projection models in Cases 1 and 2, instability issues might be anticipated in the cases of very weak geometry (for example, only the centre three stations of Fig. 4), compounded by poor initial estimates for the camera principal distance. In such circumstances, which should be avoided in normal practice, the Singular Value Decomposition (SVD) can be employed instead of inner constraint bordering in order to remove the datum defect in the normal equations (Stamatopoulos et al., 2010). The 12 smallest singular values obtained in the SVD can be disregarded, such that the pseudo-inverse of the normal equation matrix is obtained. Even though the computational cost of the SVD is very high in comparison to inner constraints, the authors' experience is that this is a very robust approach.

Case 3—Macro Lens

A network of 27 images of the surface of a 50 cent coin formed Case 3. The images were recorded, three each at nine basic camera station locations, using a Nikon D80 SLR camera with a Sigma AF 105 mm macro lens, from a distance of 40 cm. Fig. 6 illustrates the

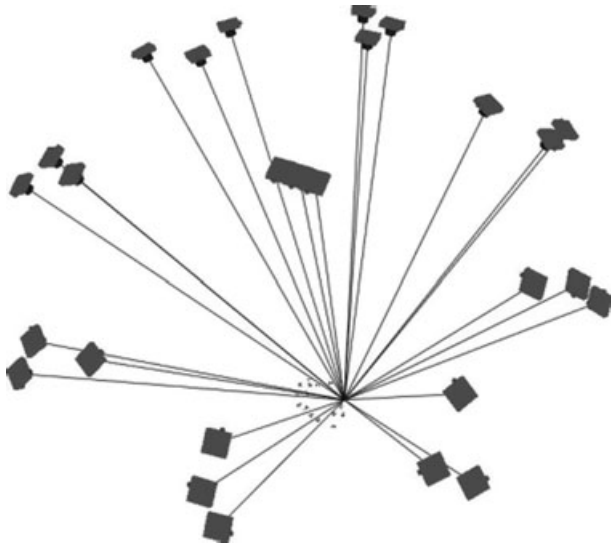

FIG. 6. Twenty-seven image network configuration for Case 3.

convergent imaging geometry employed. Since there was no focal length ring on the lens, the principal distance value could only be guessed prior to calibration from the magnification index, which was set to 1:3. The principal distance obtained in the subsequent self-calibration turned out to be 134·8 mm (field of view of approximately 10°). Seventeen coded targets comprising half millimetre diameter black dots on normal paper were placed around the object to facilitate automatic exterior orientation and self-calibration.

Even though the field of view of the macro lens was more than double that of the zoom lenses employed in Cases 1 and 2, and the network displayed a strong geometry, the conventional self-calibration model (coefficients of -1 for x_p and y_p in the **A** matrix) was unstable and produced erroneous results for interior orientation parameters. The perspective model approach with modified partial derivative terms, on the other hand, was able to reliably provide a repeatable and correct solution for the camera self-calibration. Moreover, with the resulting rms value of image coordinate residuals being 1·1 μm, the attained standard errors of object space coordinates were 1·3 μm (1:45 000) in the surface plane of the coin and 0·8 μm (1:68 000) in depth.

CONCLUDING REMARKS

Robust and reliable recovery of camera calibration parameters, and especially interior orientation elements, via self-calibration has been a long-standing problem in close range photogrammetric measurement involving long focal length lenses. The contribution of the reported research work to the alleviation of this problem has been twofold. Firstly, it has been demonstrated that much of the problem of instability in the solution of the traditional self-calibrating bundle adjustment of narrow angle photography can be attributed to an incomplete formulation of the partial derivatives of the extended collinearity equations with respect to the principal point parameters. The proposed expansion of the terms for x_p and y_p in the configuration matrix **A** will mitigate the solution instability to a considerable extent, though the perspective model can still be expected to display shortcomings, indicated by inflated variance estimates in the covariance matrix of parameters, as the field of view becomes narrower than, say, 3 to 4°. In such circumstances, which correspond in practical terms to the use of very long telephoto lenses on digital SLR cameras, the orthogonal projection model provides a viable alternative to the collinearity approach. It facilitates accurate and reliable recovery of camera parameters via a self-calibrating bundle adjustment, within a computational process that lends itself to full automation.

REFERENCES

BROWN, D. C., 1971. Close-range camera calibration. *Photogrammetric Engineering*, 37(8): 855–866.

CRONK, S., FRASER, C. S. and HANLEY, H. B., 2006. Automated metric calibration of colour digital cameras. *Photogrammetric Record*, 21(116): 355–372.

FRASER, C. S., 1982. Optimization of precision in close-range photogrammetry. *Photogrammetric Engineering and Remote Sensing*, 48(4): 561–570.

FRASER, C. S., 1984. Network design considerations for non-topographic photogrammetry. *Photogrammetric Engineering and Remote Sensing*, 50(8): 1115–1126.

FRASER, C. S. and YAMAKAWA, T., 2004. Insights into the affine model for high-resolution satellite sensor orientation. *ISPRS Journal of Photogrammetry and Remote Sensing*, 58(5–6): 275–288.

FRASER, C. S. and AL-AJLOUNI, S., 2006. Zoom-dependent camera calibration in digital close-range photogrammetry. *Photogrammetric Engineering and Remote Sensing*, 72(9): 1017–1026.

FRYER, J. G. and FRASER, C. S., 1986. On the calibration of underwater cameras. *Photogrammetric Record*, 12(67): 73–85.

HATTORI, S., ONO, T., FRASER, C. and HASEGAWA, H., 2000. Orientation of high-resolution satellite images based on affine projection. *International Archives of Photogrammetry and Remote Sensing*, 33(B3): 359–366.

LÄBE, T. and FÖRSTNER, W., 2004. Geometric stability of low-cost digital consumer cameras. *International Archives of Photogrammetry and Remote Sensing*, 35(B1): 528–534.

LUHMANN, T., ROBSON, S., KYLE, S. and HARLEY, I. A., 2006. *Close Range Photogrammetry: Principles, Techniques and Applications*. Whittles, Caithness, Scotland. 510 pages.

NOMA, T., OTANI, H., ITO, T., YAMADA, M. and KOCHI, N., 2002. New system of digital camera calibration. *International Archives of the Photogrammetry, Remote Sensing and Spatial Information Sciences*, 34(5): 54–59.

OKAMOTO, A., 1992. Ultra-precise measurement using affine transformation. *International Archives of Photogrammetry and Remote Sensing*, 29(B5): 318–322.

ONO, T. and HATTORI, S., 2002. Fundamental principles of image orientation using orthogonal projection model. *International Archives of Photogrammetry, Remote Sensing and Spatial Information Sciences*, 34(B3): 194–199.

ROVA, M., ROBSON, S. and COOPER, M. A. R., 2008. Multistation bundle adjustment with a machine vision parallel camera system—an alternative to the perspective case for the measurement of small objects. *International Archives of Photogrammetry, Remote Sensing and Spatial Information Sciences*, 37(B5): 45–50.

STAMATOPOULOS, C., FRASER, C. S. and CRONK, S., 2010. On the self-calibration of long focal length lenses. *International Archives of Photogrammetry, Remote Sensing and Spatial Information Sciences*, 38(B5): 560–564.

WILEY, A. G. and WONG, K. W., 1995. Geometric calibration of zoom lenses for computer vision metrology. *Photogrammetric Engineering and Remote Sensing*, 61(1): 69–74.

Résumé

L'un des obstacles pratiques à l'utilisation de lentilles à longue focale en photogrammétrie rapprochée est la difficulté que l'on rencontre pour l'orientation externe du réseau et de l'auto-étalonnage avec le modèle d'équations de colinéarité lorsque le champ de vue n'excède pas 10 degrés environ. Cet article présente une étude dans laquelle deux pistes ont été explorées pour l'auto-étalonnage de caméras à longue focale. La première a consisté à reconsidérer la linéarisation des équations de colinéarité avec des paramètres d'étalonnage supplémentaires en déterminant les coefficients de la matrice design correspondant aux éléments de l'orientation interne. La seconde est une nouvelle approche pour le calcul des coordonnées dans l'espace objet par l'emploi d'un modèle de projection orthogonale pouvant être formulé comme une compensation par faisceaux avec un auto-étalonnage. Des considérations de précision sont abordées pour les deux approches et des études de cas sont présentées dans lesquelles sont utilisés des télé-objectifs et des lentilles macro.

Zusammenfassung

Hindernisse für den Einsatz von Objektiven mit langer Brennweite in der Nahbereichsphotogrammetrie resultieren aus dem verwendeten Kollinearitätsmodell bei dem Schwierigkeiten bei der äußeren Orientierung des Netzwerkes und bei der Selbstkalibrierung auftreten können, wenn der Öffnungswinkel der Kamera kleiner als ungefähr 10° ist. Dieser Beitrag stellt eine Untersuchung vor, die zwei verschiedene Möglichkeiten zur Verbesserung der Selbstkalibrierung langbrennweitiger Kameras verfolgt. Die erste Möglichkeit untersucht die Linearisierung der Kollinearitätsgleichungen mit zusätzlichen Kalibrierparametern und dabei insbesondere die Bestimmung der Koeffizienten der Designmatrix im Zusammenhang mit den Elementen der inneren Orientierung. Der zweite Ansatz stellt eine neue Methode zur Berechnung von Objektkoordinaten durch Verwendung eines orthogonalen Projektionsmodells vor, das wie eine Bündelausgleichung mit Selbstkalibrierung

formuliert werden kann. Die Genauigkeitsaspekte beider Ansätze werden diskutiert und Testfälle, mit sowohl Zoom- als auch Makroobjektiven, werden vorgestellt.

Resumen

Uno de los principales impedimentos prácticos para utilizar lentes de gran distancia focal en la fotogrametría de objeto cercano es la dificultad para determinar la orientación externa de la red y la autocalibración al aplicar el modelo de ecuaciones de colinealidad cuando el ángulo de campo de la cámara es menor de unos 10°. Este artículo describe una investigación en la que se estudiaron dos vías diferentes para mejorar la autocalibración de las cámaras de gran distancia focal. La primera es una revisión de la linealización de las ecuaciones de colinealidad con parámetros de calibración adicionales, y especialmente la determinación de los coeficientes en la matriz de diseño que corresponden a los elementos de orientación interna. La segunda es una nueva perspectiva para el cálculo de las coordenadas del espacio objeto empleando un modelo de proyección ortogonal que puede denominarse ajuste por haces autocalibrante. Se discute la cuestión de la exactitud en ambas aproximaciones y se presentan ensayos empleando tanto lentes zoom como lentes macro.

APPENDIX

Expressions for Partial Derivatives Forming the Configuration Matrix **A** *Related to Camera Calibration Parameters*

$$\frac{\partial f_x}{\partial c} = \frac{(Z - Z_o)}{H} \frac{(-r_{33}x_{corr}(r_{13}x_{corr} + r_{23}y_{corr}))}{(r_{33}c - r_{13}x_{corr} - r_{23}y_{corr})^2}$$

$$\frac{\partial f_x}{\partial x_p} = \frac{(Z - Z_o)}{H} \left(\frac{r_{33}c(-1 - K_1r^2 - 2K_1(x - x_p)^2)(r_{33}c - r_{13}x_{corr} - r_{23}y_{corr})}{(r_{33}c - r_{13}x_{corr} - r_{23}y_{corr})^2} + \frac{x_{corr}(r_{13}(-1 - K_1r^2 - 2K_1(x - x_p)^2) - 2r_{23}K_1(x - x_p)(y - y_p))}{(r_{33}c - r_{13}x_{corr} - r_{23}y_{corr})^2} \right)$$

$$\frac{\partial f_x}{\partial y_p} = \frac{(Z - Z_o)}{H} \left(\frac{-2r_{33}cK_1(x - x_p)(y - y_p)(r_{33}c - r_{13}x_{corr} - r_{23}y_{corr})}{(r_{33}c - r_{13}x_{corr} - r_{23}y_{corr})^2} + \frac{x_{corr}(r_{23}(-1 - K_1r^2 - 2K_1(y - y_p)^2) - 2r_{13}K_1(x - x_p)(y - y_p))}{(r_{33}c - r_{13}x_{corr} - r_{23}y_{corr})^2} \right)$$

$$\frac{\partial f_x}{\partial K_1} = \frac{(Z - Z_o)}{H}\left(\frac{r_{33}c(x - x_p)r^2(r_{33}c - r_{13}x_{corr} - r_{23}y_{corr})}{(r_{33}c - r_{13}x_{corr} - r_{23}y_{corr})^2} + \frac{x_{corr}(r_{13}(x - x_p)r^2 + r_{23}(y - y_p)r^2)}{(r_{33}c - r_{13}x_{corr} - r_{23}y_{corr})^2}\right)$$

$$\frac{\partial f_y}{\partial c} = \frac{(Z - Z_o)}{H}\frac{(-r_{33}y_{corr}(r_{13}x_{corr} + r_{23}y_{corr}))}{(r_{33}c - r_{13}x_{corr} - r_{23}y_{corr})^2}$$

$$\frac{\partial f_y}{\partial x_p} = \frac{(Z - Z_o)}{H}\left(\frac{-2r_{33}cK_1(x - x_p)(y - y_p)(r_{33}c - r_{13}x_{corr} - r_{23}y_{corr})}{(r_{33}c - r_{13}x_{corr} - r_{23}y_{corr})^2} + \frac{y_{corr}(r_{13}(-1 - K_1r^2 - 2K_1(x - x_p)^2) - 2r_{23}K_1(x - x_p)(y - y_p))}{(r_{33}c - r_{13}x_{corr} - r_{23}y_{corr})^2}\right)$$

$$\frac{\partial f_y}{\partial y_p} = \frac{(Z - Z_o)}{H}\left(\frac{r_{33}c(-1 - K_1r^2 - 2K_1(y - y_p)^2)(r_{33}c - r_{13}x_{corr} - r_{23}y_{corr})}{(r_{33}c - r_{13}x_{corr} - r_{23}y_{corr})^2} + \frac{y_{corr}(r_{23}(-1 - K_1r^2 - 2K_1(y - y_p)^2) - 2r_{13}K_1(x - x_p)(y - y_p))}{(r_{33}c - r_{13}x_{corr} - r_{23}y_{corr})^2}\right)$$

$$\frac{\partial f_y}{\partial K_1} = \frac{(Z - Z_o)}{H}\left(\frac{r_{33}c(y - y_p)r^2(r_{33}c - r_{13}x_{corr} - r_{23}y_{corr})}{(r_{33}c - r_{13}x_{corr} - r_{23}y_{corr})^2} + \frac{y_{corr}(r_{13}(x - x_p)r^2 + r_{23}(y - y_p)r^2)}{(r_{33}c - r_{13}x_{corr} - r_{23}y_{corr})^2}\right).$$

Expressions for Partial Derivatives Forming the Configuration Matrix **B** *Related to Image Coordinate Observations*

$$\frac{\partial f_x}{\partial x} = \frac{(Z - Z_o)}{H}\left(\frac{r_{33}c(1 + K_1r^2 + 2K_1(x - x_p)^2)(r_{33}c - r_{13}x_{corr} - r_{23}y_{corr})}{(r_{33}c - r_{13}x_{corr} - r_{23}y_{corr})^2} + \frac{x_{corr}(r_{13}(1 + K_1r^2 + 2K_1(x - x_p)^2) + 2r_{23}K_1(x - x_p)(y - y_p))}{(r_{33}c - r_{13}x_{corr} - r_{23}y_{corr})^2}\right)$$

$$\frac{\partial f_x}{\partial y} = \frac{(Z - Z_o)}{H}\left(\frac{2r_{33}cK_1(x - x_p)(y - y_p)(r_{33}c - r_{13}x_{corr} - r_{23}y_{corr})}{(r_{33}c - r_{13}x_{corr} - r_{23}y_{corr})^2} + \frac{x_{corr}(2r_{13}K_1(x - x_p)(y - y_p) + r_{23}(1 + K_1r^2 + 2K_1(y - y_p)^2))}{(r_{33}c - r_{13}x_{corr} - r_{23}y_{corr})^2}\right)$$

$$\frac{\partial f_y}{\partial x} = \frac{(Z - Z_o)}{H}\left(\frac{2r_{33}cK_1(x - x_p)(y - y_p)(r_{33}c - r_{13}x_{corr} - r_{23}y_{corr})}{(r_{33}c - r_{13}x_{corr} - r_{23}y_{corr})^2} + \frac{y_{corr}(r_{13}(1 + K_1r^2 + 2K_1(x - x_p)^2) + 2r_{23}K_1(x - x_p)(y - y_p))}{(r_{33}c - r_{13}x_{corr} - r_{23}y_{corr})^2}\right)$$

$$\frac{\partial f_y}{\partial y} = \frac{(Z - Z_o)}{H}\left(\frac{r_{33}c(1 + K_1r^2 + 2K_1(y - y_p)^2)(r_{33}c - r_{13}x_{corr} - r_{23}y_{corr})}{(r_{33}c - r_{13}x_{corr} - r_{23}y_{corr})^2} + \frac{y_{corr}(2r_{13}K_1(x - x_p)(y - y_p) + r_{23}(1 + K_1r^2 + 2K_1(y - y_p)^2))}{(r_{33}c - r_{13}x_{corr} - r_{23}y_{corr})^2}\right) .$$